FORMATION MECHANISM AND SYNTHESIS OF HIGHLY CRYSTALLINE POROUS ZnO SUPERSPHERES VIA SOL-GEL PROCESS: EVOLUTION FROM INTACT HOLLOW STRUCTURES TO POLLEN-LIKE MORPHOLOGIES

The Son Le[1,*]

[1]*Faculty of Physics and Chemical Engineering, Le Quy Don Technical University, Hanoi, Vietnam*

Abstract

The synthesis of hollow and porous (HP) ZnO superspheres with intact hollow structures is crucial for various applications, yet it poses significant challenges. This article explores the fundamental aspects of preparing highly crystalline HP ZnO superspheres via a sol-gel process, elucidating the synthetic strategy, formation mechanism, and subsequent utilization for generating pollen-like ZnO superstructures. Under solvothermal conditions at 200°C, employing zinc acetate (0.065 M) in diethylene glycol with varying molar ratios of H_2O/Zn, a range of ZnO particles and superspheres were synthesized. Within a molar ratio range of 2 - 4, initial nanoparticles self-assembled into solid and porous (SP) superspheres, evolving dominantly towards or along the c-axis, resulting in HP superspheres with intact hollow structures. Conversely, molar ratios of 6 - 20 yielded only separate nanocrystals instead of superspheres. The critical role of the H_2O/Zn molar ratio in forming HP superstructures with intact hollows was highlighted, controlling Ostwald ripening and outward diffusion rates, with a molar ratio of 2 identified as a prerequisite for intact HP superspheres. The resultant intact HP superspheres exhibited intense and sharp band gap emission at 389 nm, indicating potential for optoelectronic applications. Furthermore, the study introduces pollen-like ZnO colloids derived from these intact HP ZnO superspheres, offering stable dispersion. Crystal growth predominantly occurred along the outward-oriented c-axis. The intact HP ZnO superspheres serve as a promising template system for biomimetic pollen-like ZnO superstructures.

Keywords: *ZnO; superspheres; polen-like structure.*

1. Introduction

The precise arrangement of inorganic nanobuilding units into specific sizes, compositions, phases, and morphologies is a focal point in current materials synthesis, driving the design of new materials and devices with diverse optical, electrical, magnetic, catalytic, and other properties. Notably, the assembly of nanobuilding units into hollow and porous (HP) superspheres has garnered significant interest for their applications in functional materials. Zinc oxide (ZnO), with its wide band-gap (3.37 eV) and large

* Email: sonlt@lqdtu.edu.vn
DOI: 10.56651/lqdtu.jst.v2.n01.776.pce

excitation binding energy (60 meV), has spurred synthesis and application studies for HP superspheres due to their unique properties in catalysts, sensors, actuators, photovoltaic devices, and biomedicines [1-5]. The properties of HP ZnO superspheres depend heavily on factors such as morphology, aspect ratio, size, orientation, and density of the nanobuilding units, or nanocrystallites. While templating is effective for preparing HP ZnO superspheres, careful control of the interface between the template and nanobuilding units is essential [6-9]. However, using sacrificial templates complicates the removal process without affecting the nanocrystals and HP superstructures. Alternatively, template-free syntheses of HP ZnO superspheres have been developed utilizing sol-gel-derived solvothermal or hydrothermal reactions, which offer neat, cost-effective methods requiring relatively simple equipment [7-12]. However, HP ZnO superspheres prepared via sol-gel-derived solvothermal or hydrothermal reactions often exhibit cracks, a common occurrence even with alternative preparation methods [7, 10, 12]. The presence of cracks in HP ZnO superspheres is problematic for delivery purposes and for utilizing specific crystalline facets, as both the interior and exterior surfaces are exposed evenly to the medium [13-15]. Therefore, synthesizing highly crystalline HP ZnO superspheres without cracks has been challenging but important. Additionally, understanding the fundamental formation mechanism of HP superspheres is crucial. HP ZnO superspheres with intact hollows (i.e., without cracks) hold potential for various applications, including as delivery vesicles, catalysts, optoelectronic devices, and as templates for biomimetic pollen-like or urchin-like colloids, which represent a three-dimensional assembly of one-dimensional building units and have garnered significant attention for their biomimetic structures and unique physical properties [13, 15-18].

After a thorough review, we concluded that the cracked openings in HP ZnO superspheres may result from harsh reaction conditions during the hollowing process. Therefore, in this study, we explore the fundamental conditions necessary to prepare sol-gel-derived highly crystalline HP ZnO superspheres. Additionally, we present the synthetic strategy and mechanism for producing HP ZnO superspheres with intact hollows. Furthermore, we showcase the derivation of pollen-like ZnO colloids from these HP ZnO superspheres with intact hollows, illustrating the neat three-dimensional assembly of one-dimensional nanocrystallites.

2. Experiments

2.1. Chemicals

Zinc acetate ($Zn(CH_3CO_2)_2$, Sigma Aldrich, 99.99%), diethylene glycol (DEG, Sigma Aldrich, 99%). All chemicals were of analytical purity, with no further purification required.

2.2. Syntheses of HP ZnO superspheres with/without cracked openings

Zinc acetate (0.46 g, 2.5 mmol) was mixed with 40 mL of DEG and deionized water

(DW), with the molar ratio of H_2O to Zn varied from 20 to 10, 6, 4, 3, and 2. A ratio of 2 was determined as the minimum for complete dissolution of zinc acetate after vigorous stirring and intermittent sonication. The mixture (~35 mL) was transferred to a 45-mL Teflon-lined autoclave and heated to 200°C for 12 hours or various time periods. After cooling, the solution was mixed with 35 mL of ethanol and centrifuged. The resulting solid product was washed with ethanol and dispersed in 20 mL of ethanol to create a stock solution. For solid-state characterization, a portion of the stock solution was centrifuged and the solid was dried in an oven at 60°C for 3 hours. The samples were labeled according to the molar ratio of H_2O/Zn used for their synthesis, as sample 20, 10, 6, 4, 3, and 2, for convenient comparison.

2.3. Growth of HP ZnO superspheres to pollen-like ones

A 0.9 M NaOH aqueous solution (10 mL) was added to a zinc acetate solution (0.050 g in 5 mL of DW) while stirring. Within 5 minutes, 5 mL of HP ZnO superstructure solution (8 mg/mL in DW) was added with continuous stirring. To prevent agglomeration, the HP ZnO aqueous solution was freshly prepared from the stock solution via centrifugation and dispersion in DW without undergoing a drying process. The resulting mixture solution was transferred to a 45-mL Teflon-lined autoclave and treated in an oven at 80°C for 12 hours. The product was washed with ethanol and water using centrifugation and then dispersed in 20 mL of ethanol.

2.4. Material characterizations

High-resolution transmission electron microscopy (HR-TEM) images were captured using a Technai F20 G2 (FEI, 200 kV) or TITAN TEM (FEI, 300 kV). Scanning electron microscopy (SEM) images were acquired with an FEI Inspect F50 at 15 kV after the samples were coated with Pd/Pt by ion sputtering for 20 seconds (HITACHI, E-1010). X-ray diffraction (XRD) patterns were recorded using a Rigaku Dmax 2500 with Cu-Kα radiation (λ =1.5406 Å). The nanocrystallite size was determined from X-ray line broadening using the Scherrer formula. Photoluminescence (PL) spectra of solid samples were obtained at room temperature using a 15 mW He-Cd CW laser (IK3151R-E, KIMMON KOHA) for excitation at 325 nm. For solid sample preparation, the sample solution was deposited on a silicon wafer and allowed to dry naturally. PL spectra of solution samples were measured using a Hitachi F-7000 spectrophotometer with 325 nm excitation, maintaining a ZnO concentration of 0.12 mg/mL in all traces, with ethanol as the solvent. The Brunauer-Emmett-Teller (BET) surface area and porosity were determined from N_2 adsorption and desorption isotherms using a micromeritics ASAP-2010 at -196°C. Prior to measurement, samples were degassed at 100°C for 1 hour.

3. Results and discussions

As previously mentioned, HP ZnO superspheres prepared via sol-gel-derived solvothermal or hydrothermal reactions often exhibit cracked openings. Additionally, these superspheres typically possess relatively large diameters (ranging from 1 to 4 μm) and large nanocrystal building units (ranging from 20 to 60 nm) compared to the size of gel particles (~10 nm) [11, 12, 19-21]. In sol-gel-derived reactions, the formation of solid and porous (SP) ZnO superspheres (Scheme 1a) initially occurs through the self-assembly of amorphous gel particles or poorly crystalline particles, aiming to reduction of their surface energy. The building unit particles in these SP superstructures adopt various orientations [11, 20-23]. Subsequently, different hollowing mechanisms have been proposed under various reaction conditions, often resulting in cracked openings in the micrometer-sized superspheres. For instance, Wang et al. [11] suggested a self-assembled secondary SP supersphere followed by a successive yolk/shell-type intermediate, while Tian et al. [21] proposed a solid twin-microsphere intermediate derived from the primary SP superspheres, eventually transforming into HP superspheres. In this study, we propose retaining the primary SP superspheres without further assembly and controlling their hollowing process to create intact hollows. This is achieved through a combined effect of Ostwald ripening and directional diffusion outward (Scheme 1a-b-d), akin to the Kirkendall effect observed in metal corrosion processes [24-26]. In the case of SP ZnO superspheres, ZnO gels or poorly crystalline particles dissolve at the core, diffuse outward, and contribute to crystal growth near the exterior surface, while voids diffuse inward through the porous wall as illustrated in Scheme 1b. This outward diffusion process needs to be carefully controlled during the hollowing process to prevent premature eruption through weaker or thinner parts of the porous wall, resulting in cracked openings like Scheme 1c [11, 21]. To synthesize HP ZnO superspheres with intact hollows like Scheme 1d, a mild and slow hollowing process must be implemented, as further discussed later in this study.

The sol-gel-derived solvothermal or hydrothermal reaction is a one-pot process conducted in an autoclave. The sol-gel process of Zn^{2+} ions necessitates water and a base catalyst to facilitate hydrolysis and condensation reactions [21, 27-29]. Therefore, our synthetic approach aimed to minimize the use of water and base catalyst to maintain a mild and gradual process. It was decided to employ the solvothermal reaction with polyol (DEG) instead of the hydrothermal reaction using water as the solvent. The solvothermal reaction temperature was set at 200°C to ensure high crystallinity. Anhydrous zinc acetate was selected as the Zn precursor, and the molar ratio of H_2O to Zn was varied to establish the optimal range for HP superspheres. No additional base catalyst was introduced

because acetate anions released from the Zn precursor can act as a base catalyst by reacting with H_2O, generating OH^-, which subsequently contributes to the formation of $Zn(OH)_2$ and ZnO through hydrolysis and condensation reactions [17, 29]. Initially, efforts were made to determine the highest soluble concentration of zinc acetate in DEG. Without H_2O, the solubility of zinc acetate in DEG was insufficient for practical synthesis. Upon adding H_2O with a molar ratio of $H_2O/Zn = 2$, the highest concentration of zinc acetate in DEG was found to be 0.0625 M after prolonged vigorous stirring for 3 hours with intermittent sonication. Therefore, the concentration of zinc acetate was standardized at 0.0625 M for all reactions.

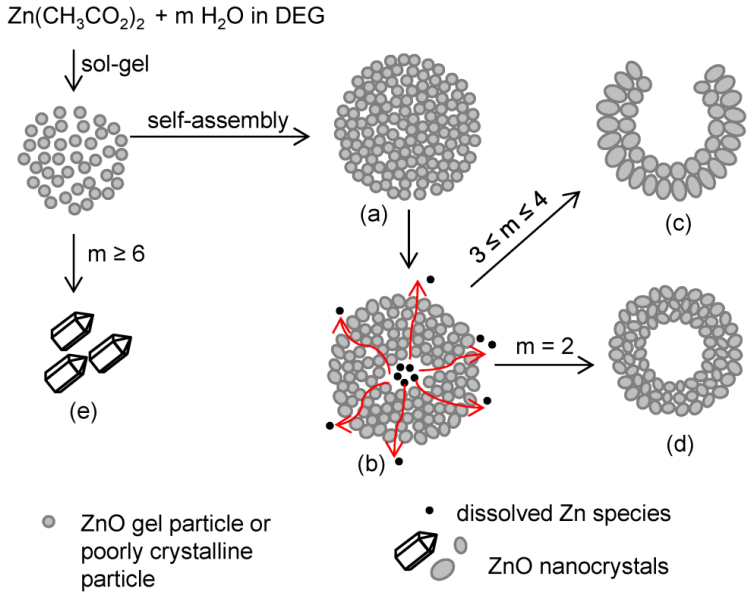

Scheme 1. Schematic representation of the proposed mechanism for formation of hollow and porous (HP) ZnO superspheres; (a) self-assembled solid and porous (SP) supersphere, (b) hollowing intermediate, (c) cracked open HP supersphere, (d) intact HP supershpere, and (e) separated ZnO nanocrystals. 'm' denotes the molar ratio of H_2O/Zn.

SEM images of ZnO products obtained at a molar ratio of H_2O/Zn equal to or greater than 6 are depicted in Fig. S1. No superstructure formation via self-assembly is observed. As the molar ratio increases from 6 to 10 and 20, the dimensions of representative crystals (highlighted by yellow circles) increase from approximately 51 nm × 97 nm to 51 nm × 141 nm and 61 nm × 222 nm, respectively, exhibiting an evolution towards a hexagonal pencil-like shape. This crystal growth behavior aligns with previous findings indicating preferential growth along the c-axis of wurtzite ZnO in reactions with the plentiful water [20, 21, 27-32]. Under the current solvothermal conditions, with a fixed Zinc acetate concentration (2 equivalents based on Zn) and varying water content

(≥ 6 equivalents based on Zn), initially formed ZnO gel particles can undergo crystallization and dissolution to yield $[Zn(OH)_4]^{2-}$. This transformation process is accelerated in solutions with higher molar ratios of H_2O/Zn. $[Zn(OH)_4]^{2-}$ is recognized as the primary chemical species promoting crystal growth along the c-axis in wurtzite ZnO. Consequently, crystallization of nanogel and subsequent crystal growth via Ostwald ripening occur relatively faster with increasing water content. As a result, the resulting crystallite size increases proportionally with the molar ratio. These crystals attain a sufficient size, and their concentrations are relatively low, thus obviating the need for superstructure formation to reduce surface energy within the molar ratio range of H_2O/Zn = 6 - 20, yielding free particles as depicted in the SEM images of Fig. S1.

The first column of Fig. 1 showcases SEM images of ZnO products with the molar ratios of 2, 3, and 4. In these instances, the nanogel building units are densely packed due to their relatively slow crystallization and growth rates, resulting in the formation of SP superspheres through self-assembly to minimize surface energy. Subsequently, crystallization and hollowing processes ensue. Most of the hollows exhibit cracks at molar ratios 3 and 4, while the majority remain intact at the molar ratio of 2, underscoring the pivotal role of water in the concurrent processes of Ostwald ripening and outward diffusion. These features are delineated in Scheme 1, with 'm' denoting the molar ratio of H_2O/Zn. The diameters of HP ZnO superspheres within molar ratios 2 and 3 fall within a similar range of 310 - 770 nm, slightly larger for molar ratio 4. The inset SEM image of each HP ZnO supersphere provides a magnified view, obtained from as-prepared samples for molar ratios 3 and 4, and via mechanical cracking to observe the interior for molar ratio 2. As the molar ratio increases from 2 to 4, the nanocrystal building units become coarser and larger, the porous wall thinner, and the hollow larger. Enhanced water content promotes dissolution of the core material, with the dissolved solution diffusing out through the porous wall at molar ratio 2, and additionally expanding and erupting through weaker sections, leading to cracked openings at molar ratios 3 and 4. The diffused or erupted solution facilitates crystal growth near the supersphere surface. TEM images on the right side of Fig. 1 corroborate the hollow nature of the superspheres, evident from the comparatively brighter core parts contrasted with the wall parts, consistent with SEM observations. Although the assembled nanocrystals appear crowded in TEM images, HRTEM images near the exterior surface reveal discernible nanocrystal morphologies. With increasing molar ratio from 2 to 3 and 4, exterior surface nanocrystals exhibit morphological evolution from oval to elongated oval shapes, outward of HP ZnO superspheres, with approximate nanocrystal diameter (nm) × length (nm) from 17 × 23 to 20 × 36 and 21 × 42, respectively.

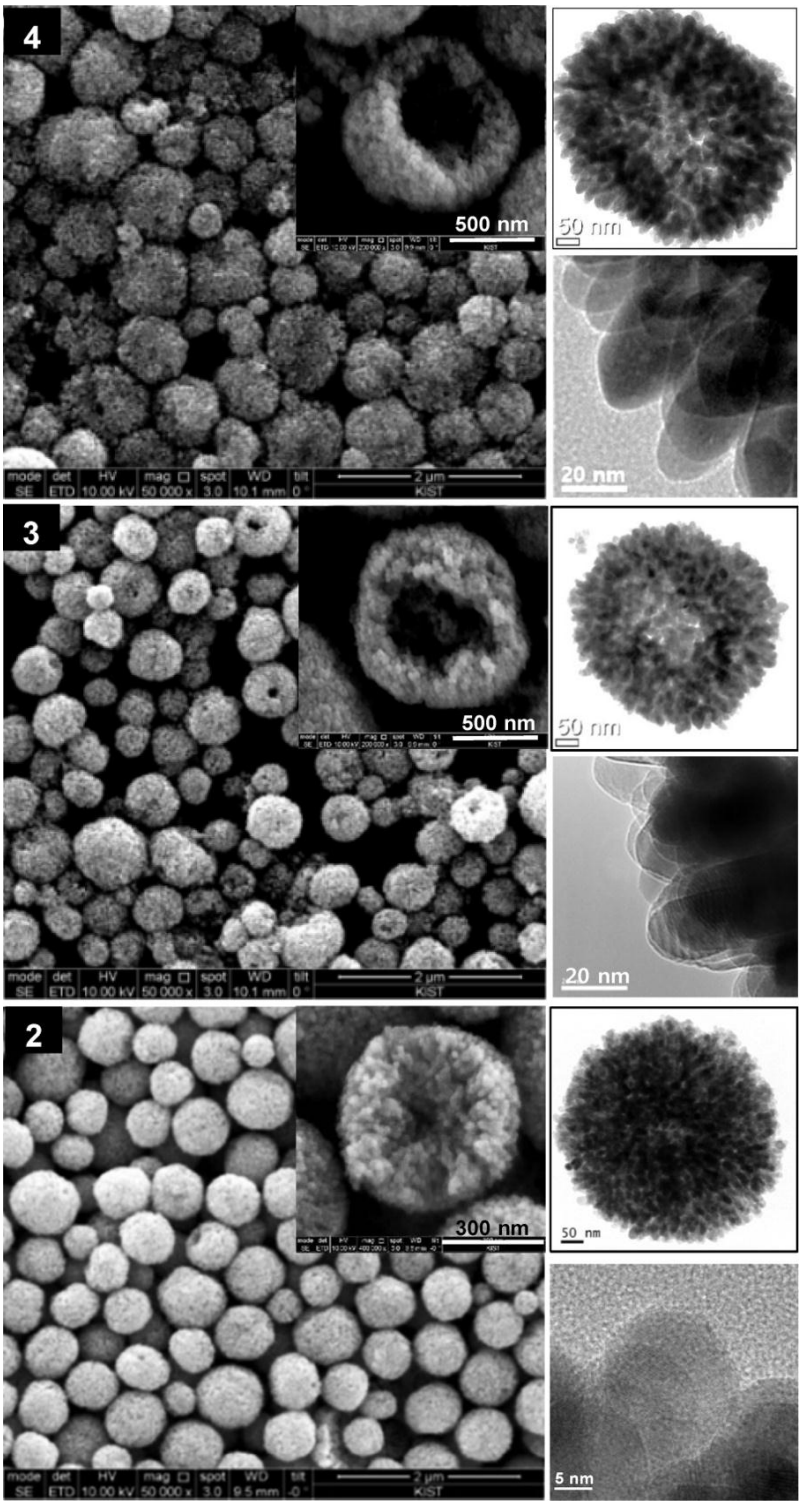

Fig. 1. SEM, magnified SEM, TEM, and HRTEM images (clockwise direction) of HP ZnO superspheres synthesized with molar ratio H_2O/Zn of 4, 3, and 2.

To explore the crystalline orientations of nanocrystals within the superstructure, numerous HRTEM images of the exterior surfaces of sample 4 were captured. Additionally, Fourier-transformed electron diffraction (ED) patterns for the marked areas were obtained and depicted alongside their cropped images in Fig. S2. Along the exterior surface of the ZnO supersphere, nanocrystals predominantly display growth directions aligned with the c-axis (Fig. S2 c-e), or a shift in growth direction towards the c-axis (Fig. S2 b). This suggests that although the initial nanoparticles assembled in various orientations within the supersphere, subsequent crystal growth predominantly occurred outward along the c-axis. Further discussion on this analysis will be provided in relation to Fig. 5 later on.

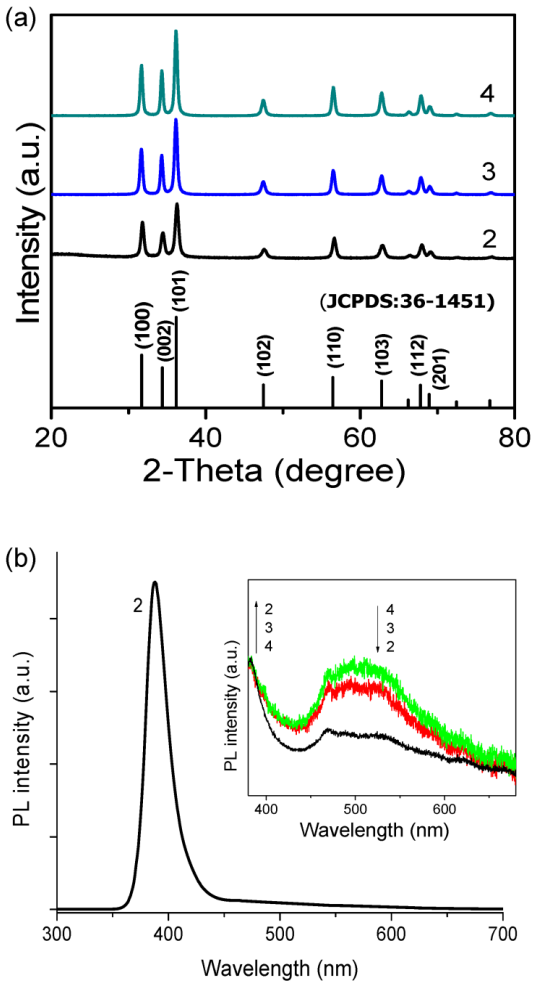

Fig. 2. (a) XRD patterns and (b) PL spectrum of HP ZnO superspheres synthesized with molar ratio of H_2O/Zn, 4, 3, and 2. Inset of (b) indicates PL spectra at colloidal solution state.

Figure 2a depicts the XRD patterns of the HP ZnO supersphere series, all of which exhibit a highly crystalline wurtzite structure, as confirmed by the standard JCPDS file

No. 36-1451. The relative diffraction intensity of (100)/(002) for isotropic ZnO typically yields a value of 1.17, and any deviations from this value indicate an anisotropic crystal growth [22, 33, 34]. As the molar ratio of H_2O/Zn increases from 2 to 3 and 4, the relative diffraction intensity of (100)/(002) decreases from 1.33 to 1.15 and 1.12, respectively. This suggests that the longer crystalline direction of sample 2 is perpendicular to the c-axis, differing from samples 3 and 4. The relative diffraction intensity of (100)/(002) in samples 3 and 4 suggests slightly elongated crystals along the c-axis, consistent with the HRTEM image analysis (Fig. S2) where we proposed that initial nanoparticles assembled with different orientations, but later preferred crystal growth occurred along the c-axis, outward of the superspheres. This differently oriented assembly of initial nanoparticles and subsequent preferred growth along the c-axis appears consistent across all HP supersphere samples in the current system, with a decreasing growth rate as the molar ratio of H_2O/Zn decreases. However, the crystal growth rate is significantly slower when the water amount is limited with a molar ratio of 2. Further discussion on the crystal growth of sample 2 will be provided later with Fig. 3-5. The crystallite sizes of nanobuilding units estimated from X-ray line broadening, assuming spherical nanocrystals, are 17 nm, 20 nm, and 21 nm for samples with molar ratios of 2, 3, and 4, respectively, consistent with the exterior nanocrystallite diameters obtained from HRTEM images (Fig. 1). However, the crystallite lengths obtained from HRTEM images exhibit some discrepancies from those obtained from XRD (23 nm, 36 nm, and 42 nm vs. 17 nm, 20 nm, and 21 nm, respectively, for samples with molar ratios of 2, 3, and 4). This can be attributed to morphological differences and the preferential crystal growth at the exterior surface compared to the inner part of a supersphere, as illustrated in Scheme 1c and d. The XRD data provide an average size assuming spherical nanocrystallites, whereas the HRTEM data offer a representative size of the exterior nanocrystallites, which can be larger than the inner nanocrystallites of a supersphere according to the proposed mechanism.

Figure S3 presents the photoluminescence (PL) spectra of all synthesized ZnO samples in ethanol. Inset in Fig. 2b displays selected PL spectra for HP ZnO suspensions with molar ratios of 2, 3 and 4. The band at 380 - 400 nm and the broad band at 450 - 600 nm correspond to the band gap and oxygen defect of ZnO nanocrystals, respectively [12]. As the molar ratio of H_2O/Zn decreases, the PL intensity due to oxygen defect decreases, while the relative PL intensity of band gap vs. oxygen defect increases, consistent with other reports [12, 35]. Hence, it can be inferred that higher water content generates more oxygen defects through rapid crystal growth. Conversely, the minimum water amount is a prerequisite condition for wurtzite ZnO with minimal oxygen defects. The solid-state PL

spectrum of HP ZnO superspheres with a molar ratio of 2 is depicted in Fig. 2b, where the sharp and strong band gap peak at 389 nm (3.19 eV) indicates high quality of its optical property.

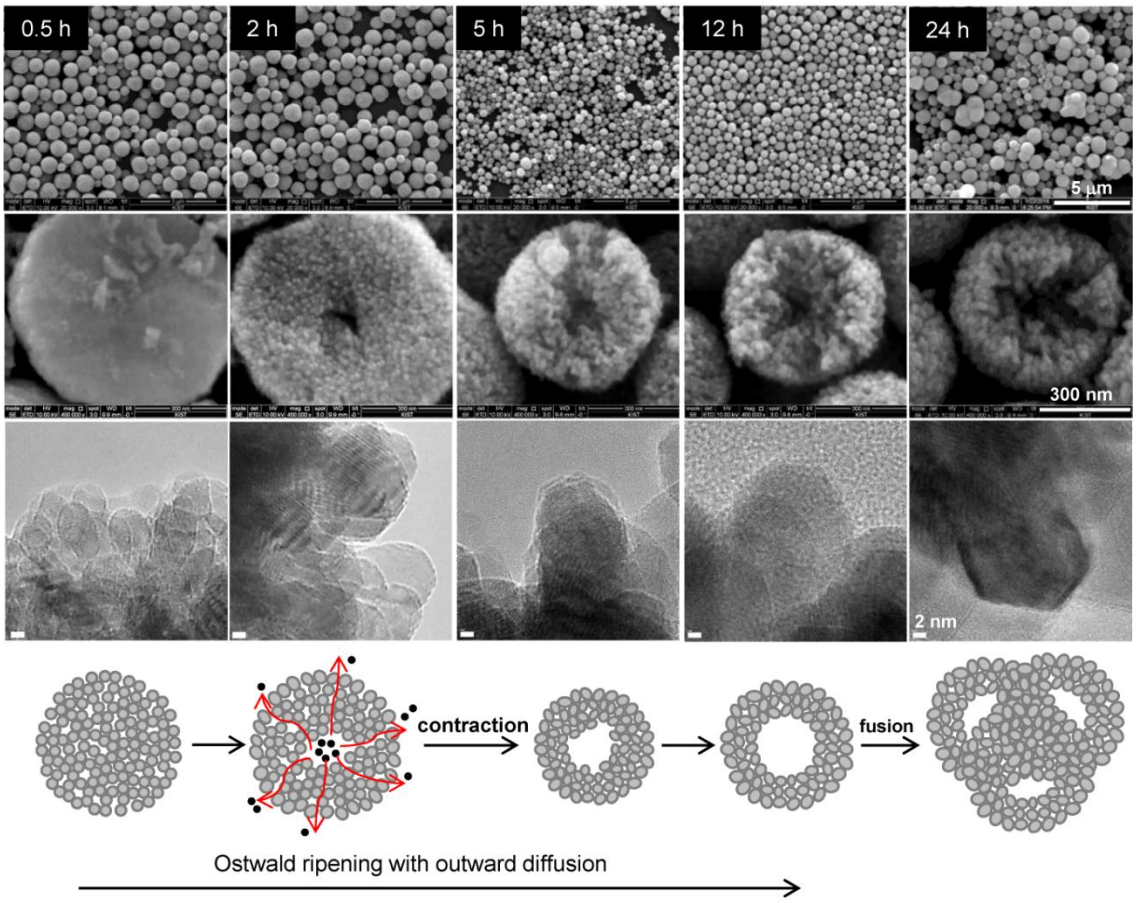

Fig. 3. SEM, magnified SEM, and HRTEM images (exterior surface) and schematic representation (from top to bottom) showing temporal evolution of intact HP ZnO superspheres with molar ratio of H_2O/Zn = 2. Scale bar on the rightmost side fits for each row.

Figures 3 and 4 depict the SEM/HRTEM images and XRD patterns of ZnO superspheres or their exterior surface nanobuilding units with a molar ratio of H_2O/Zn = 2, illustrating their hollowing process in a solvothermal reactor at 200 °C. To observe the interior part of each supersphere, the samples were mechanically cracked, and their SEM images are displayed in the second row of Fig. 3. The proposed hollowing mechanism illustration is redrawn with a detailed addition of a contraction step. At 0.5 h, SP ZnO superspheres with diameters of 500 - 1200 nm are formed by the self-assembly of ~10 nm-sized nanogel building units. Although poorly crystallized (XRD), crystallization of assembled

nanogels is evident, showing oval-shaped nanoparticles at the exterior surface of the superspheres (HRTEM). By 2 h, further crystallization of nanoparticles occurs, accompanied by the dissolution of core materials, outward diffusion, and consumption for nanocrystal growth of the exterior part. This combined process of Ostwald ripening and outward diffusion results in enlarged hollows and pores in the superspheres. After 5 h, the loosely structured HP superspheres contract, yielding denser and smaller HP superspheres with diameters of 250 - 730 nm. Subsequent reaction leads to an increase in both the size of surface nanocrystallites and the diameter of HP ZnO superspheres. The sample after 12 h exhibits the best controlled quality in terms of size distribution (average ± standard deviation = 529 ± 126 nm for 200 particles) and crystallinity. However, further reaction beyond 12 h causes the superspheres to fuse together, yielding diversely sized products (320 - 2050 nm). The diameters of crystallites constructing the superspheres were calculated from the Scherrer equation and X-ray line broadening, with respective values of 9.7, 12.8, 13.3, 16.8, and 19.8 nm for 0.5, 2, 5, 12, and 24 h samples, reasonably agreeing with the representative short diameters (9.3, 11.6, 13.3, 18.4, and 18.7 nm respectively) obtained from the HRTEM images in Fig. 3. The relative diffraction intensity of (100)/(002) in Fig. 4 exhibits a temporal decrease from 1.52 to 1.49, 1.37, and 1.33 until 12 h, indicating relatively preferred crystal growth toward the c-axis, although the diameter along the c-axis is still relatively shorter than that along the a-axis. After 24 h, the relative diffraction intensity of (100)/(002) increases to 1.39, suggesting a new crystal growth behavior related to the fusion of the HP superspheres, as displayed in the SEM image of Fig. 3.

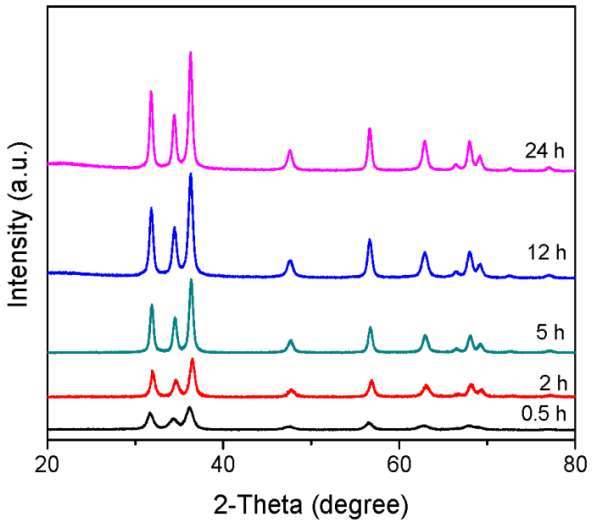

Fig. 4. Temporal XRD patterns during synthesis of intact HP ZnO superespheres with molar ratio of H_2O/Zn = 2.

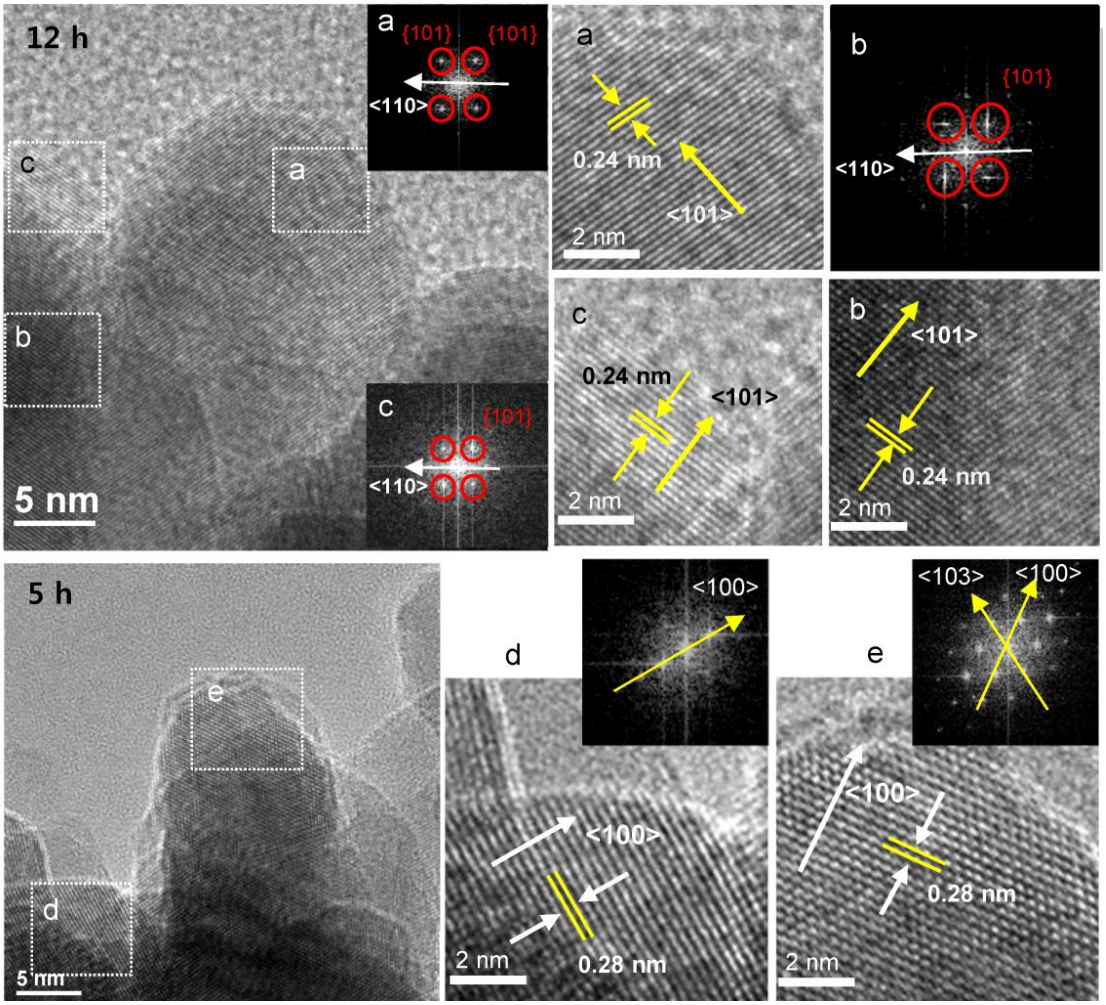

Fig. 5. Selected HRTEM images, and ED patterns and cropped HRTEM images for the dotted areas during synthesis of intact HP ZnO superspheres with molar ratio of H_2O/Zn = 2.

The nanoparticles on the HP superspheres with a molar ratio of 2 exhibited poor crystallinity in their early stages (0.5 h and 2 h) and were densely packed, making it challenging to discern their growth directions in the HRTEM images (Fig. 3). Subsequently, the samples at 5 h and 12 h displayed improved crystallinity. HRTEM images of their exterior surfaces and Fourier transformed ED patterns for the dotted areas were obtained and presented with their cropped images in Fig. 5. At 5 h, the nanocrystals exhibited oval shapes, with the long diameter oriented along the a-axis (Fig. 5 a) or growing toward the c-axis (Fig. 5 b). By 12 h, the nanocrystals displayed oval shapes, with the long diameters growing toward the c-axes (<2$\bar{1}$1> directions).

This suggests that the initial nanocrystals, with long diameters along the a-axes, were assembled in different orientations, but later, their growth occurred preferentially toward the c-axes, outward of the superspheres. If fusion does not occur, the nanocrystals will continue to grow along the c-axes, as observed in sample 4. However, fusion between the flattened facets from other superspheres resulted in permanent aggregation (Fig. 3).

In summary, it is proposed that gel particles or poorly crystalline particles assemble into SP superspheres to minimize their surface energy through various interactions such as dipole-dipole interaction, van der Waals force, and hydrogen bonding, consistent with the suggestion by Barick et al. [23]. Under the current solvothermal conditions, further crystallization primarily occurs from the exterior surface of the superspheres, with a gradient in crystallization rate decreasing towards the core due to the more readily available ingredients for crystallization and growth at the exterior. The core of the supersphere, being relatively poorly crystalline, is preferentially dissolved, diffused out, and utilized for crystal growth near the exterior surface in a controlled manner for sample 2, whereas it proceeds in an uncontrolled manner for samples 3 and 4. The growth of exterior crystals is believed to be driven by $[Zn(OH)_4]^{2-}$ species diffusing out from the core, depositing preferably on (001) crystal surfaces due to the termination of Zn and O ions on these surfaces, resulting in effectively positive and negative polarization in wurtzite ZnO. Consequently, relative crystal growth occurs along the c-axis, with only nanocrystals whose c-axes are oriented outward able to continue growing, while others will be spatially confined. This outward crystal growth mechanism is facilitated by the porous nature of the superspheres, which is retained throughout their lifecycle. Indeed, the N_2 gas adsorption-desorption isotherm of sample 2 (Fig. S4) exhibits a typical type IV curve, indicating a predominance of mesopores. The BET surface area and corresponding Barrett-Joyner-Halenda (BJH) pore volume were determined to be 46 m^2/g and 0.217 cm^3/g, respectively, with predominant mesopores ranging from 6 to 50 nm in diameter, peaking at 24 nm. These values indicate relatively high surface area and porosity, consistent with SEM and TEM images. They are greater and similar, respectively, to the reported values of 20.6 m^2/g and 0.22 cm^3/g for self-aggregated solid and porous ZnO superspheres synthesized through a soft chemical route [23].

Based on the XRD and SEM/HRTEM analyses presented in Figures 3-5, it has been inferred that the nanoparticles initially crystallize with a long diameter along the a-axis and later experience growth toward or along the c-axis, predominantly outward from the HP superspheres, although some may exhibit tilting. If this holds true, a pollen-like supersphere should be readily obtainable via hydrothermal reaction from the HP supersphere with an intact hollow (sample 2), considering the highly preferential crystal growth along the c-axis compared to the a- or b-axis [13, 36]. However, deriving a neatly formed pollen-like structure from cracked-open HP superspheres (sample 3 or 4) is unlikely due to the differing interior crystalline orientations, allowing dominant crystal growth even within the cracked hollow, as confirmed in Fig. S5. Pollen-like ZnO superspheres were obtained via hydrothermal reaction of sample 2 with zinc acetate and NaOH. Their SEM images, showcasing various magnifications, are displayed on the left side of Fig. 6a. To observe the interior part of the pollen-like supersphere, the sample was mechanically cracked, and its SEM image is displayed on the right side of Fig. 6a. The pollen-like superspheres retain an intact hollow structure, are well-dispersed without aggregation, and notably, exhibit predominant outward growth of exterior nanocrystals. The length of one-dimensional nanocrystals assembled on the surface of the supersphere is approximately 300 nm, and the predominant growth of wurtzite ZnO nanocrystals along the c-axes is evident in the XRD pattern of Fig. 6b, reflected in the reversed peak intensity of (002) over (100), contrasting with the JCPDS file No. 36-1451 in Fig. 2a. The TEM/HRTEM images of the pollen-like supersphere, displayed in Fig. 7 along with Fourier transformed ED patterns and marked c-axes, confirm outward crystal growth along the crystalline c-axes from the exterior surface of the supersphere. The PL spectrum of the pollen-like supersphere in Fig. 6c is compared with that of sample 2 in Fig. 2b. As expected from rapid crystal growth under ample water and base catalyst, the band gap peak at 389 nm drastically decreases, and the broad band at 450-650 nm becomes relatively prominent, indicating a relatively high presence of oxygen defects in the one-dimensional nanocrystallites constructing the pollen-like supersphere. It appears that the exterior nanobuilding units play a critical role in determining the optoelectronic properties of a supersphere.

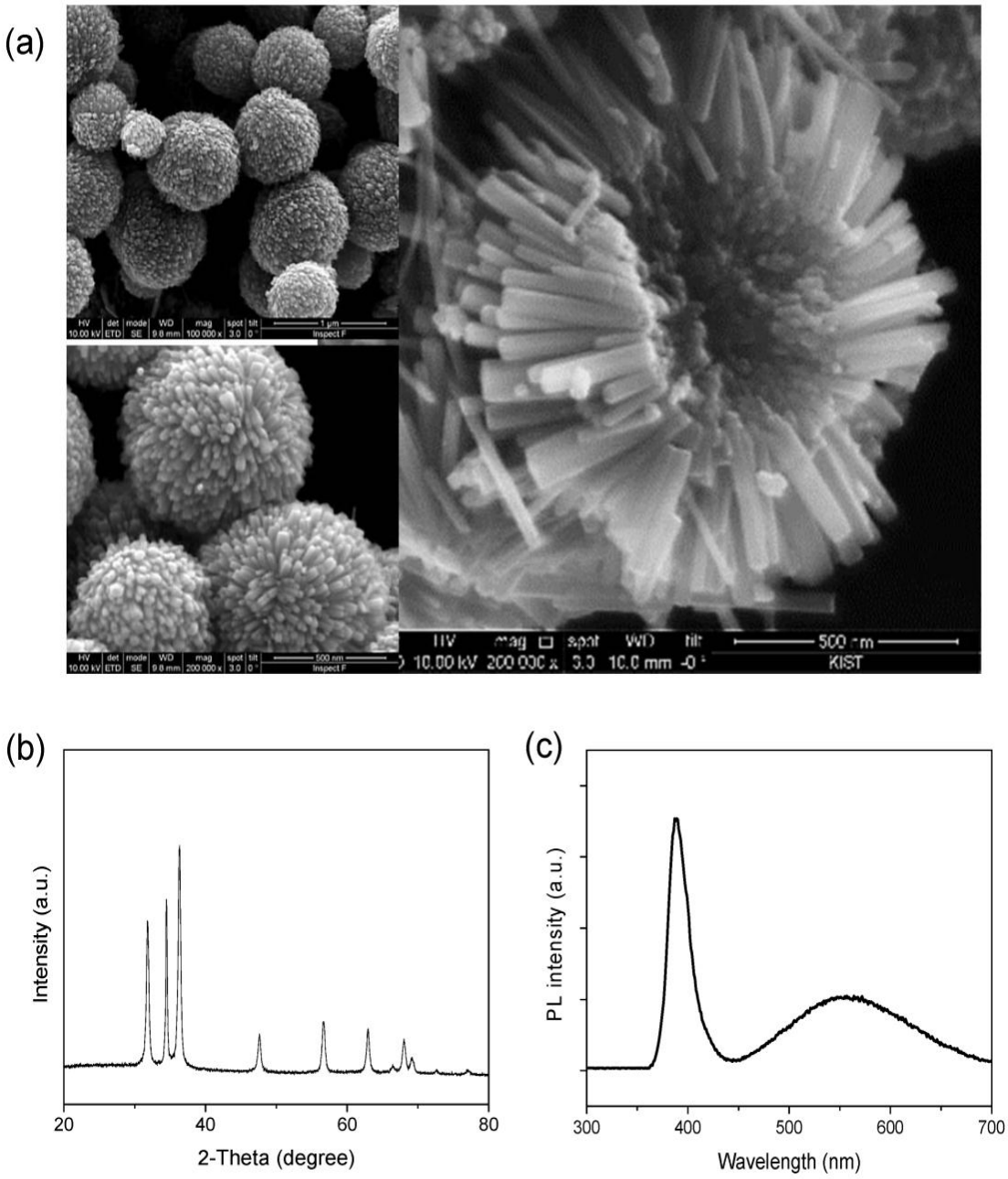

Fig. 6. (a) SEM images with different magnifications, (b) XRD pattern, and (c) PL spectrum of pollen-like ZnO superstructures.

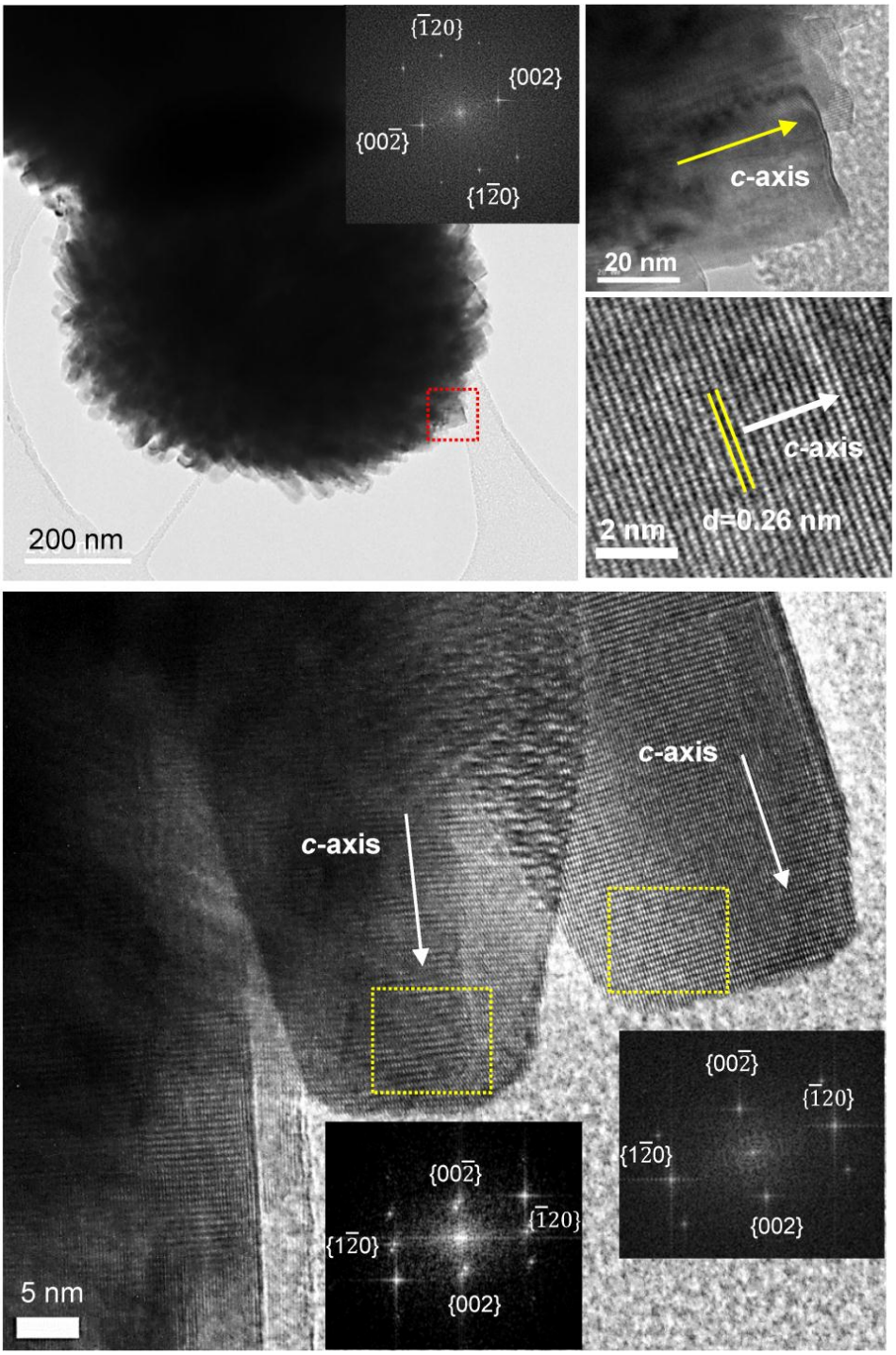

Fig. 7. TEM and HRTEM images of pollen-like ZnO superstructure and its edges, and ED patterns for the dotted areas.

4. Conclusion

Overall, this study presented a fundamental investigation into the preparation of sol-gel-derived highly crystalline HP ZnO superspheres, along with the synthetic strategy and formation mechanism of HP ZnO superspheres featuring intact hollows. The critical role of the molar ratio of H_2O/Zn in the solvothermal system was highlighted, particularly in achieving HP superstructures with intact hollows by controlling the rates of Ostwald ripening and outward diffusion. It was found that a molar ratio of 2 was necessary for the formation of intact HP superspheres. Within the molar ratio range of 2-4, the initial nanoparticles exhibited self-assembly in various orientations to form SP superspheres, followed by preferential growth along or toward the c-axis. Leveraging this property, pollen-like ZnO colloids were successfully derived from the intact HP ZnO superspheres through a hydrothermal reaction. Such intact HP superspheres hold potential as model systems for biomimetic superstructures resembling pollen-like or urchin-like structures. Ongoing research is focused on exploring the applications of the synthesized materials, with findings to be reported in subsequent publications.

References

[1] S. R. Kelly et al., "ZnO as an Active and Selective Catalyst for Electrochemical Water Oxidation to Hydrogen Peroxide", *ACS Catalysis*, Vol. 9 (5), pp. 4593-4599, 2019.

[2] Y. Kang et al., "Review of ZnO-based nanomaterials in gas sensors", *Solid State Ionics*, Vol. 360, 2021, 115544.

[3] Y. Li et al., "Ultrathin flexible linear-piezoelectric ZnO thin film actuators: Tuning the piezoelectric responses by in-plane epitaxial strain", *Applied Surface Science*, Vol. 599, 2022, 153969.

[4] C. Otalora, M. A. Botero, and G. Ordoñez, "ZnO compact layers used in third-generation photovoltaic devices: A review", *Journal of Materials Science*, Vol. 56 (28), pp. 15538-15571, 2021.

[5] A. Yadav, K. Mondal, and A. Gupta, "Biomedical application of ZnO nanoscale materials", in *Metal Oxides for Biomedical and Biosensor Applications*, K. Mondal (Editor), Elsevier, 2022, pp. 407-435.

[6] F. Caruso, R. A. Caruso, and H. Möhwald, "Nanoengineering of Inorganic and Hybrid Hollow Spheres by Colloidal Templating", *Science*, Vol. 282 (5391), pp. 1111-1114, 1998.

[7] H. C. Zeng, "Synthesis and self-assembly of complex hollow materials", *Journal of Materials Chemistry*, Vol. 21 (21), pp. 7511-7526, 2011.

[8] C. C. Yec and H. C. Zeng, "Synthesis of complex nanomaterials via Ostwald ripening", *Journal of Materials Chemistry A*, Vol. 2 (14), pp. 4843-4851, 2014.

[9] X. Wang et al., "Synthesis, Properties, and Applications of Hollow Micro-/Nanostructures", *Chemical Reviews*, Vol. 116 (18), pp. 10983-11060, 2016.

[10] J. Yu and X. Yu, "Hydrothermal Synthesis and Photocatalytic Activity of Zinc Oxide Hollow Spheres", *Environmental Science & Technology*, Vol. 42 (13), pp. 4902-4907, 2008.

[11] L. Wang et al., "Facile synthesis of ZnO hollow microspheres and their high performance in photocatalytic degradation and dye sensitized solar cells", *Journal of Alloys and Compounds*, Vol. 647, pp. 57-62, 2015.

[12] J. Yin et al., "Water Amount Dependence on Morphologies and Properties of ZnO nanostructures in Double-solvent System", *Scientific Reports*, Vol. 4 (1), 2014, 3736.

[13] B. Liu and H. C. Zeng, "Fabrication of ZnO "Dandelions" via a Modified Kirkendall Process", *Journal of the American Chemical Society*, Vol. 126 (51), pp. 16744-16746, 2004.

[14] X. Li et al., "Template-free microwave-assisted synthesis of ZnO hollow microspheres and their application in gas sensing", *CrystEngComm*, Vol. 15 (15), pp. 2949-2955, 2013.

[15] G. Shen, Y. Bando, and C. J. Lee, "Synthesis and Evolution of Novel Hollow ZnO Urchins by a Simple Thermal Evaporation Process", *The Journal of Physical Chemistry B*, Vol. 109 (21), pp. 10578-10583, 2005.

[16] J. Elias et al., "Hollow Urchin-like ZnO thin Films by Electrochemical Deposition", *Advanced Materials*, Vol. 22 (14), pp. 1607-1612, 2010.

[17] J. Seo et al., "Preparation of Highly Monodisperse Electroactive Pollen Biocomposites", *ChemNanoMat*, Vol. 2 (5), pp. 414-418, 2016.

[18] G. Zan and Q. Wu, "Biomimetic and Bioinspired Synthesis of Nanomaterials/Nanostructures", *Advanced Materials*, Vol. 28 (11), pp. 2099-2147, 2016.

[19] Y. F. Zhu, D. H. Fan, and W. Z. Shen, "Template-Free Synthesis of Zinc Oxide Hollow Microspheres in Aqueous Solution at Low Temperature", *The Journal of Physical Chemistry C*. Vol. 111 (50), pp. 18629-18635, 2007.

[20] T. Ihara et al., "Template-free solvothermal preparation of ZnO hollow microspheres covered with c planes", *RSC Advances*, Vol. 4 (48), pp. 25148-25154, 2014.

[21] S. Tian et al., "Hierarchical ZnO hollow microspheres with exposed (001) facets as promising catalysts for the thermal decomposition of ammonium perchlorate", *CrystEngComm*, Vol. 17 (45), pp. 8689-8696, 2015.

[22] S. Singh, K. C. Barick, and D. Bahadur, "Shape-controlled hierarchical ZnO architectures: photocatalytic and antibacterial activities", *CrystEngComm*, Vol. 15(23), pp. 4631-4639, 2013.

[23] K. C. Barick et al., "Self-Aggregation and Assembly of Size-Tunable Transition Metal Doped ZnO Nanocrystals", *The Journal of Physical Chemistry C*, Vol. 112 (39), pp. 15163-15170, 2008.

[24] R. W. Balluffi and B. H. Alexander, "Relative Diffusion Rates of Zinc and Copper in Alpha Brass", *JOM*, Vol. 4 (12), pp. 1315-1316, 1952.

[25] Y. Yin et al., "Formation of Hollow Nanocrystals Through the Nanoscale Kirkendall Effect", *Science*, Vol. 304 (5671), pp. 711-714, 2004.

[26] X. Liang et al., "Formation of CeO_2–ZrO_2 Solid Solution Nanocages with Controllable Structures via Kirkendall Effect", *Journal of the American Chemical Society*, Vol. 130 (9), pp. 2736-2737, 2008.

[27] Z. Hui et al., "Synthesis of flower-like ZnO nanostructures by an organic-free hydrothermal process", *Nanotechnology*, Vol. 15 (5), 2004, 622.

[28] F. Xu et al., "Synthesis and Photoluminescence of Assembly-Controlled ZnO Architectures by Aqueous Chemical Growth", *The Journal of Physical Chemistry C.*, Vol. 113 (3), pp. 1052-1059, 2009.

[29] J. Zhan et al., "A novel synthesis and excellent photodegradation of flower-like ZnO hierarchical microspheres", *CrystEngCom*, Vol. 15 (47), pp. 10272-10277, 2013.

[30] C. Ye et al., "Zinc Oxide Nanostructures: Morphology Derivation and Evolution", *The Journal of Physical Chemistry B*, Vol. 109 (42), pp. 19758-19765, 2005.

[31] R. Shi et al., "Growth of flower-like ZnO via surfactant-free hydrothermal synthesis on ITO substrate at low temperature", *CrystEngComm*, Vol. 14 (18), pp. 5996-6003, 2012.

[32] Y. Su et al., "Microstructure, growth process and enhanced photocatalytic activity of flower-like ZnO particles", *RSC Advances*, Vol. 6(9), pp. 7403-7408, 2016.

[33] A. McLaren et al., "Shape and Size Effects of ZnO Nanocrystals on Photocatalytic Activity", *Journal of the American Chemical Society*, Vol. 131 (35), pp. 12540-12541, 2009.

[34] S. S. Kanmani and K. Ramachandran, "Role of aqueous ammonia on the growth of ZnO nanostructures and its influence on solid-state dye sensitized solar cells", *Journal of Materials Science*, Vol. 48 (5), pp. 2076-2091, 2013.

[35] X. Sun et al., "ZnO Twin-Cones: Synthesis, Photoluminescence, and Catalytic Decomposition of Ammonium Perchlorate", *Inorganic Chemistry*, Vol. 47 (10), pp. 4146-4152, 2008.

[36] Y. Bao, C. Wang, and J. Z. Ma, "A two-step hydrothermal route for synthesis hollow urchin-like ZnO microspheres", *Ceramics International*, Vol. 42 (8), pp. 10289-10296, 2016.

CƠ CHẾ HÌNH THÀNH VÀ TỔNG HỢP CÁC SIÊU CẤU TRÚC ZnO TINH THỂ CAO BẰNG PHƯƠNG PHÁP SOL-GEL: QUÁ TRÌNH BIẾN ĐỔI TỪ CẤU TRÚC VI CẦU RỖNG ĐẾN HÌNH THÁI HỌC DẠNG HOA

Lê Thế Sơn[1]

[1]*Khoa Hóa - Lý kỹ thuật, Trường Đại học Kỹ thuật Lê Quý Đôn, Hà Nội, Việt Nam*

Tóm tắt: Các siêu cầu ZnO rỗng và xốp (HP) với cấu trúc nguyên vẹn có ứng dụng trong nhiều lĩnh vực khác nhau. Tuy nhiên, việc tổng hợp vật liệu như vậy gặp rất nhiều khó khăn. Nghiên cứu này góp phần vào việc tối ưu hóa quy trình điều chế siêu cầu HP ZnO với độ kết tinh cao bằng phương pháp sol-gel, đề xuất cơ chế hình thành và khả năng sử dụng các siêu cầu HP ZnO để tạo ra ZnO dạng cấu trúc hình hoa với cấu trúc 3D phức tạp hơn. Trong điều kiện phản ứng nhiệt dung môi ở 200°C, bằng cách sử dụng zinc acetate (0,065 M) trong diethylene glycol với các tỉ lệ mol H_2O/Zn khác nhau, đã tổng hợp được một loạt vật liệu ZnO ở dạng hạt kích thước nanomet và dạng siêu cầu. Trong phạm vi tỉ lệ mol 2 - 4, các hạt nano ban đầu tự tập hợp thành các siêu cầu rắn và xốp (SP), phát triển chủ yếu về phía hoặc dọc theo trục c, tạo ra các siêu cầu HP với cấu trúc rỗng nguyên vẹn. Ngược lại, tỉ lệ mol 6 - 20 chỉ tạo ra tinh thể nano riêng biệt thay vì siêu cầu. Vai trò quan trọng của tỉ lệ mol H_2O/Zn trong việc hình thành cấu trúc 3D HP với các lỗ rỗng nguyên vẹn đã được chỉ rõ. Tỉ lệ này góp phần kiểm soát tốc độ của quá trình chín Ostwald và tốc độ khuếch tán ra bên ngoài. Tỉ lệ mol H_2O/Zn = 2 được xác định là điều kiện tiên quyết để có được các siêu cầu HP nguyên vẹn. Các siêu cầu này phát xạ mạnh và sắc nét ở 389 nm, cho thấy các ứng dụng quang điện tiềm năng. Ngoài ra, nghiên cứu cũng xem xét việc sử dụng các siêu cầu ZnO HP nguyên vẹn để tổng hợp ZnO cấu trúc 3D dạng hoa có khả năng phân tán ổn định. Quá trình phát triển tinh thể được kiểm soát để xảy ra chủ yếu dọc theo trục c hướng ra ngoài.

Từ khóa: *ZnO; siêu cầu; vi cầu rỗng.*

Received: 08/04/2024; Revised: 10/05/2024; Accepted for publication: 20/05/2024

❑